Icarus 251 (2015) 112–127

Contents lists available at ScienceDirect

Icarus

journal homepage: www.elsevier.com/locate/icarus

The origin, evolution, and trajectory of large dust storms on Mars during Mars years 24–30 (1999–2011)

Huiqun Wang [a,*], Mark I. Richardson [b]

[a] Smithsonian Astrophysical Observatory, Cambridge, MA 02138, USA
[b] Ashima Research, Pasadena, CA 91101, USA

ARTICLE INFO

Article history:
Available online 14 November 2013

Keywords:
Mars
Mars, atmosphere
Image processing

ABSTRACT

Mars Daily Global Maps (MDGM) derived from the Mars Global Surveyor (MGS) Mars Orbiter Camera (MOC) and Mars Reconnaissance Orbiter (MRO) Mars Color Imager (MARCI) are used to study the distribution and evolution of large dust storms over the period from Mars years 24–30 (1999–2001). Large storms are defined here as discrete dust events visible in image sequences extending over at least 5 sols (Mars days) and where the dust covers areas beyond the origination region. A total of 65 large dust storms meeting these criteria are identified during the observational period and all are observed during the L_s = 135–30° seasonal window. Dust storms originating in the northern and southern hemispheres appear to form two distinct families. All but two of the storms originating in the northern hemisphere are observed in two seasonal windows at L_s = 180–240° and L_s = 305–350°; while all but two of those originating in the southern hemisphere are observed during L_s = 135–245°.

None of the large dust storms originating in the northern hemisphere are observed to develop to global scale, but some of them develop into large regional storms with peak area $>1 \times 10^7$ km^2 and duration on the order of several weeks. In comparison, large dust storms originating in the southern hemisphere are typically much smaller, except notably in the two cases that expanded to global scale (the 2001 and 2007 global storms).

Distinct locations of preferred storm origination emerge from the dust storm image sequences, including Acidalia, Utopia, Arcadia and Hellas. A route (trajectory) 'graph' for the observed sequences is provided. The routes are highly asymmetric between the two hemispheres. In the south, for non-global dust storms, the main routes are primarily oriented eastwest, whereas in the north, the routes are primarily north–south and zonally-concentrated into meridional channels. In a few impressive cases, storms originating in the northern hemisphere are observed to "flush" through Acidalia and Utopia, across the equator, and then branch in the low- and mid-southern latitudes. The origin of the 2007 global dust storm is ambiguous from the imaging data. Immediately prior to the global storm, a dust storm sequence from Chryse is identified. This storm's connection to the explosive expansion observed to start from Noachis/West Hellas is unclear due to image coverage. This paper further identifies and describes three different styles of dust storm development, which we refer to as "consecutive dust storms", "sequential activation" and "merging." The evolution of a given dust storm sequence can exhibit different combinations of these growth styles at different stages of development. Dust storm sequences can overlap in time, which makes them good candidate to grow into larger scale.

1. Introduction

Dust strongly interacts with the martian atmospheric circulation. It absorbs solar radiation and absorbs/emits in the infrared, affecting atmospheric thermal structure and dynamics. The relative importance and precise nature of dust lifting mechanisms remain uncertain, but wind stresses associated with motions on scales from regional to microscale (convective) are likely crucial (Kahn et al., 1992; Newman et al., 2002). The observed dust activity in the martian atmosphere span a wide size range from dust devils to local, regional and planet-encircling dust storms. Only the largest of these storms are observable from the Earth (Martin and Zurek, 1993). Martin and Zurek (1993) classified dust storms with long axis >2000 km as non-local dust storms which included regional and planet-encircling dust storms. Cantor et al. (2001) defined regional dust storms in Mars Global Surveyor (MGS) Mars Observer Camera (MOC) images as those with areas greater than 1.6×10^6 km^2 and lifetimes of more than 3 martian days (hence

* Corresponding author. Address: MS 50, 60 Garden Street, Cambridge, MA 02138, USA.
E-mail address: hwang@cfa.harvard.edu (H. Wang).

0019-1035/$ - see front matter © 2013 Elsevier Inc. All rights reserved.
http://dx.doi.org/10.1016/j.icarus.2013.10.033

forth referred to as "sols"). Episodic planet-encircling dust storms cover contiguous latitudinal bands and can sometimes develop into global scale (the definition of a "global dust storm" becomes a somewhat arbitrary semantic issue). Large-scale (large regional and global) dust storms last for weeks to months and have significant impact on global atmospheric structure and circulation (Martin and Richardson, 1993; Smith et al., 2002; Wang et al., 2003; Cantor, 2007; Strausberg et al., 2005; Wang, 2007). Previous studies show that a large-scale dust storm results from the aggregation of many smaller dust storms or (equivalently, depending on the definition of the word "storm") from the activation of many different dust-lifting centers (Martin and Zurek, 1993; Cantor et al., 2001; Strausberg et al., 2005; Cantor, 2007; Wang, 2007; Hinson and Wang, 2010; Hinson et al., 2012).

While prior studies have been able to identify the quasi-periodicity of global storms (Martin and Zurek, 1993), the telescopic record is not of sufficient spatial resolution to determine the "climatology" of their smaller precursor events. Developing an understanding of the "life-cycle" of these precursor storms is important for a few reasons: (1) While the limited observations to date suggest that large-scale dust storms develop from smaller ones, we do not yet have an empirical or descriptive understanding of why some storms grow and some do not. (2) The field of atmospheric modeling is now at a stage where a variety of dust storm types can be simulated (i.e. emerge) in numerical models (Newman et al., 2002; Toigo et al., 2002; Basu et al., 2006; Hollingsworth and Kahre, 2010; Mulholland et al., 2013). (3) The global observations of Mars from MGS and Mars Reconnaissance Orbiter (MRO) have been ongoing with only brief breaks since the early northern summer of Mars year 24 (1999). As such, with almost 7 martian years of global imaging completed, we are now at a point where a first attempt at a climatological survey of large-scale dust storm origin and evolution is statistically worthwhile.

In this study, we address the following important questions:

- Are there statistical groupings of dust storm sequences that form large dust storm families?
- Are there differences in the seasonality of the families?
- Where do the large dust storm families originate?
- How do large dust storms evolve and do they tend to move from specific source regions and if so, to where?

Strong constraints on the range of all possible progenitors of global storms remains beyond the scope of current data sets as only two global events have been captured so far.

In this paper, we use the Mars Daily Global Map (MDGM) products derived from MGS MOC (Wang and Ingersoll, 2002) and MRO Mars Color Imager (MARCI) wide-angle camera global map swaths. The period examined covers portions of Mars years 24–30 (1999–2011). In order to study large-scale dust storm evolution, we focus on storms that last for at least 5 sols and involve dust transport and/or lifting in regions beyond their origination areas. We will call the resulting selected data sets "dust storm sequences," with an individual dust storm sequence of MDGM images corresponding to each individual large-scale dust storm identified in Mars years 24–30 period. Examples will be shown in Section 5. The vast majority of the storms we study have peak areas $>1.6 \times 10^6$ km^2, satisfying the Cantor et al. (2001) criteria for a regional dust storm, although a few are slightly smaller (but still on the order of 10^6 km^2). Since the identified sequences cover areas beyond their origination region, they have the potential to grow larger. Two of the 65 cases identified grew into global dust storms.

Each dust storm sequence we examined involved multiple lifting sites with various sizes and lifetimes. The association of these lifting centers with an individual large dust storm is thus retrospective in the analysis. By our definition, the evolution of a dust storm sequence involved one or more active lifting centers on each day, generated a cumulative dusty area involving several connected regions, and had a continuous development history and a well-defined route for travel. Within a sequence, a subsequent dust lifting event could initiate either in the original initiation region or along the route of an earlier event, and subsequent dust clouds within a storm sequence could then either continue along the same direction as its predecessor or turn in a different direction. This multiple, parallel and dynamic character of large dust storms not only presents a challenge for individual storm categorization, but appears to be sufficiently ubiquitous a trait of large dust storms that it would need to be reproduced by any successful model. It should be noted that more than one sequence can overlap in time (see Section 5). Consequently, there are cases when some dust storms contribute to one sequence while others contribute to another on the same day. When metrics such as the area for each sequence is calculated, it is done separately on the basis of our judgment of dust storms as being part of the same sequence or not.

Dust storms occur frequently in the circumpolar latitudes and many qualify as regional dust storms (Cantor et al., 2001; Cantor, 2007; Wang, 2007; Wang et al., 2011). If we were to define a "dust storm sequence" purely in terms of dustiness over an extended period of time, it would be difficult to decide whether to group the observed circumpolar events into one season-long "dust storm" or many shorter dust storm sequences. A further complication of the analysis of polar storms is that the winter polar night obviously cannot be imaged in the visible wavelengths. Therefore, we have excluded circumpolar dust storms from this study unless they show substantial equator-ward motion and growth outside of the polar region. This is not to diminish the importance of circumpolar storms as it should be noted that these storms are amongst the most frequently observed forms of dust activity on Mars (Cantor et al., 2001; Cantor, 2007; Liu et al., 2003) and "seed" the development of many larger storms we observe outside of the polar region (and which we then do include in our study when they grow and migrate in such cases).

For the limiting extreme of global dust storms, all dust lifting activity at all locations may be considered to comprise a single dust storm sequence based on our definition. However, as described in Strausberg et al. (2005) and Cantor (2007), there were many distinct dust lifting centers that persisted for weeks during different stages of the 2001 global dust storm and it is not clear how these centers related to one another. In particular, it is not clear how the presence or absence of a global storm would modify the "normal" development of large-scale dust storm (such as that seeded by the northern frontal storms). Given that dramatic changes in the global mean atmospheric opacity likely significantly modify the background circulation of the atmosphere, we make no attempt to interpret or include separate dust storm sequences during either of the two global dust storms. However, it should be noted that such sequences could be identified.

It should also be noted that in this study we do not include short-lived storms or events that remain localized – this exclusion stems directly from our definition of the problem: we seek to address how to large-scale dust storms grow, evolve, and migrate. Common areas of isolated and/or short-lived storms include the Hellas basin and the Arcadia/Amazonis region to the northwest of Tharsis. In assessing all the MDGMs, we note that these seemingly random and isolated short-lived events can occur at many locations. The majority should probably be considered as local events, as cataloged by Cantor et al. (2001) and Cantor (2007), even through some may have exceeded prior area-based definition of local storms. However, in our selection of events we believe that we have included all candidate events from Mars years 24–30 that have the potential to grow into major dust storms.

In this paper, we initially describe the MDGM product, extending the prior application of global mosaic creation from MGS MOC wide-angle images to the MRO MARCI dataset. In Section 3, we describe the seasonal evolution of dust storm sequences, including the seasonality of storm area, northern versus southern hemisphere storm origin, and the nature of dust lifting events (especially the importance of frontal development). In Section 4, we discuss the evolutionary pathways or geographical "routing" of the storms observed in the image sequences. In Section 5, we describe the distinct families of storm development styles that emerge, the occurrences of sequence overlap and their relationship to large-scale dust storms, and the origin and evolution of the 2007 global dust storm. Finally, in Section 6 we provide a summary of results.

2. Data sets

The basic dataset used in this study is the Mars Daily Global Map archive that now extends from $L_s \approx 150°$ in Mars year 24 to $L_s = 360°$ in Mars year 30. The archive includes processed images from two separate orbiter camera systems – the entire MGS MOC set and the MRO MARCI set collected until late 2011. Each map in the MDGM archive is a mosaic of up to 13 separate global image swaths taken on a given sol by MOC (Mars years 24–28, at 2 PM) or MARCI (Mars years 28–30, at 3 PM). Consecutive MDGMs usually overlap by one orbit. A MDGM is thus not a snapshot, but represents a daily view of Mars, in the early-to-mid afternoon local time, gradually built up by the cameras. While this method can miss rapid processes (on timescales less than a sol), the dust storm sequences that are the focus of this study are well observed in MDGMs due to their large extents and long lifetimes.

The procedure for making MDGM mosaics from the MGS MOC wide-angle images was described in detail in Wang and Ingersoll (2002). The image processing for MDGM creation from MRO MARCI wide-angle images follows approximately the same steps. MARCI is a "push frame" wide-angle camera with 2 UV (260 and 320 nm) and 5 visible filters (425, 550, 600, 650 and 725 nm), taking 1–10 km/pixel images at about 3 PM local time during each orbit (Bell et al., 2009). We first use the USGS Integrated Software for Images and Spectrometers (ISIS, isis.astrogeology.usgs.gov) to perform radiometric calibration and calculate the geometry and position of each pixel. ISIS currently uses the gain and offset state listed in the image label, which corresponds to the value at the beginning of the image. However, the gain sometimes changes during an image, leading to some uncorrected gain jumps. We have recently coded our own radiometric calibration program in IDL based on the description in the "marcical.txt" file that accompanies each MARCI volume downloaded from the Planetary Data System (PDS, psd-imaging.jpl.nasa.gov). Our program automatically takes into account the possible gain changes listed in the "varexp.tab" table. Our new code also calculates the incidence angle, emission angle, phase angle, latitude and longitude of each pixel using functions from the Navigation and Ancillary Information Facility (NAIF) ICY toolkit and SPICE kernels (naïf.pds.nasa.gov). This IDL-based code has begun to be used for processing the images toward the end of the third MARCI mapping year (Mars year 30).

In the next step, we correct the vertical streaks due to pixel-to-pixel variation in each image using a normalized correction frame. Each line of the correction frame is derived from the average of the corresponding lines in the middle third of the image. Then, we use Eq. (1) with the parameter values in Table 1 to photometrically "flatten" the image to minimize large-scale brightness variations. This equation is modified from the one used for MGS MOC image processing in Wang and Ingersoll (2002), which is, in turn, similar to Hapke's bi-directional surface reflectance function (Hapke, 1986). The parameter values were derived using the average of about 100 randomly selected MARCI images in mission sub-phase B06 (February 2009). B06 was used as our reference since it was the first batch of MARCI images we processed. As a result, the photometric correction works better for some images than others. New parameter values may need to be derived for other time periods. For simplicity, however, we have applied a single set of parameter values (Table 1) throughout the processing.

$$r(i,e,g,x) = \frac{\mu_0}{\mu+\mu_0}\cdot H(\gamma,\mu_0)\cdot H(\gamma,\mu)\cdot [f\cdot G(k_1,g)+(1-f)\cdot G(k_2,g)]\cdot\left[1+\frac{B_0}{1+h_1\cdot\tan(g/2)}\right]\cdot(a_0+a_1x+a_2x^2+a_3x^3+a_4x^4) \quad (1)$$

where i is incidence angle, e is emission angle, g is phase angle, x is the pixel number along each line of the image, $\mu_0 = \cos(i)$, $\mu = \cos(e)$, $H(\gamma,\mu) = (1+2\mu)/(1+2\gamma\mu)$, $G(k,g) = (1-k^2)/(1+k^2+2k\cos(g))^{3/2}$ is the Henyey–Greenstein phase function. Parameters used in this paper are listed in Table 1. They should be updated as needed. For photometric correction, each radiometrically calibrated pixel is divided by the value of $r(i,e,g,x)$ calculated using Eq. (1).

For each color band, we mosaic 13 (or the maximum number of swaths available for a given sol if some are missing) images for each filter into a daily global map (90°S–90°N, 180°W–180°E, 0.1° × 0.1°). The pixels in the overlap areas are created from the weighted averaging of the pixels of the contributing images. Larger weights are prescribed for the pixels with a smaller sum of incidence, emission and phase angles in order to blend in. Consecutive MDGMs usually overlap by one image swath. Finally, we combine 3 MARCI visible bands (usually Band 1, 3 and 5 – blue, orange, and NIR) to form a color MDGM. An example MARCI MDGM is shown in Fig. 1.

We have visually inspected the currently available MOC and MARCI MDGMs to identify and catalog dust storm sequences. We have focused on the area between 60°S and 60°N. Our catalog contains information on the solar longitude (L_s) at the beginning and end of each sequence, the surface area apparently covered by thick dust (that completely obscures the surface) on each sol during the sequence, whether the sequence originates in the southern or northern hemisphere, and whether it involves any curvilinear shaped "frontal" structure (Wang et al., 2005). We have studied the spatial, temporal and size distributions of these dust storm sequences. We have also summarized their routes and development styles.

To provide auxiliary information, we also use selected temperature and/or optical depth data derived from the MGS Thermal Emission Spectrometer (TES, Smith, 2004), Mars Odyssey THermal EMission Imaging System (THEMIS, Smith, 2009) and MRO Mars Climate Sounder (MCS, Kleinboehl et al., 2009). The version 2 TES and version 2 MCS derived data products were downloaded from the Planetary Data System website (atmos.pds.nasa.gov) Mars archive page. The gridded THEMIS data were provided by Michael D. Smith (personal communication).

3. Seasonality

3.1. Temporal distribution

Fig. 2 shows the L_s of occurrence and duration of dust storm sequences identified in the MDGMs for Mars years 24–30. Missing data periods for each year are indicated by blanks. Each sequence is indicated by a left bracket, with the vertical line corresponding to the L_s at the beginning of the sequence and the other two sloped lines corresponding to the duration of the sequence. Each sequence is also indicated by a filled bar.

Table 1
Parameters used in Eq. (1) for photometric correction of MARCI visible images.

	γ	k_1	k_2	f	B_0	h_1	a_0	a_1	a_2	a_3	a_4
Band 1	1.5	0.368	0.0	0.6907	1.248	8.9	0.2036	0.	0.	0.	0.
Band 2	0.725	0.808	−0.0145	0.833	0.879	4.695	0.466	0.	0.	0.	0.
Band 3	0.55	0.757	−0.001	0.834	1.718	1.865	0.306	0.	0.	0.	0.
Band 4	0.40	0.822	−0.0217	0.826	0.744	2.426	0.476	0.	0.	0.	0.
Band 5	0.33	0.76	−0.0216	0.75	0.611	5.0	0.36	0.	0.	0.	0.

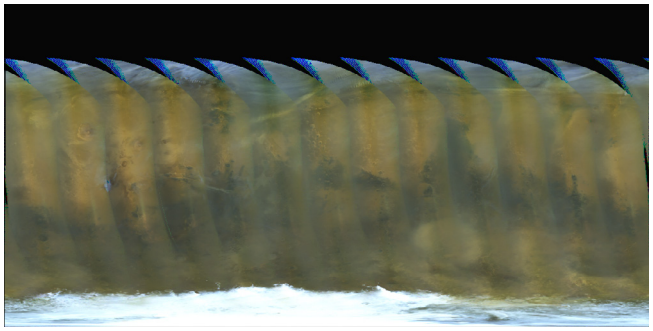

Fig. 1. Example MRO MARCI Mars Daily Global Map ($L_s \sim 239.5°$ in Mars year 30) in simple cylindrical projection (90°S–90°N, 0.1° × 0.1°).

This figure shows the generally excellent coverage provided by the two camera systems over the observational period. It also provides a good visual sense of the relative occurrence of dust storms originating in the northern (black) and southern (green) hemispheres. Our designation of a given event being a "northern hemisphere" or "southern hemisphere" sequence is based solely on the origination of the first dust storm of the sequence (which we interpret as being the "seed" or origination event); the designation does not provide information on where the dust storm or other lifting centers are located later in the sequence. Thus a dust storm originating in the northern hemisphere that is observed to lead to subsequent dust lifting in or transport to the southern hemisphere (e.g. Wang et al., 2003; Cantor, 2007) is still designated as a "northern hemisphere"-originating event.

The global dust storms that started at $L_s \sim 180°$ in Mars year 25 (2001) and at $L_s \sim 260°$ in Mars year 28 (2007) correspond to the long green bars and brackets in Fig. 2. They cover the initiation, peak and initial decay phases of the global dust storms. It should be noted that dust haze continued to decay after the periods indicated in Fig. 2. So, the lengths of the bars and brackets do not cover the whole lifetimes of the global dust storms. Since the analysis relies on an operators' subjective judgment on the border and thickness of a dust storm, it is difficult to tell when a global haze has cleared to the normal background condition. We therefore do not provide an end L_s for a global dust storm here. The 2001 global dust storm originated from west Hellas (Smith et al., 2002; Strausberg et al., 2005; Cantor, 2007). As will be shown in Section 5, the 2007 global dust storm was immediately preceded by a dust storm traveling from Chryse to Margaritifer Terra and probably reaching Noachis Terra. It is unclear how this Chryse storm is related to the 2007 global storm, for which continuous lifting began between Hellas and Noachis (Section 5). As such, the 2007 global dust storm is colored green in Fig. 2, indicating a southern-hemisphere origin.

Fig. 2 shows that dust storm sequences are most frequently observed during $L_s \sim 130–250°$ and $L_s \sim 305–350°$. During $L_s \sim 250–300°$, there is only a single case: the 2007 global dust storm in Mars year 28. No dust storm sequences are identified in the MDGMs during $L_s \sim 40–130°$. During $L_s \sim 0–40°$, there are only two cases, one originating in Acidalia in the northern hemisphere in Mars year 26 and the other in Solis/Bosporus in the southern hemisphere in Mars year 28. In general agreement with previous results (Martin, 1986; Martin and Zurek, 1993; Liu et al., 2003), Fig. 2 suggests that the northern spring and summer are relatively free of large dust

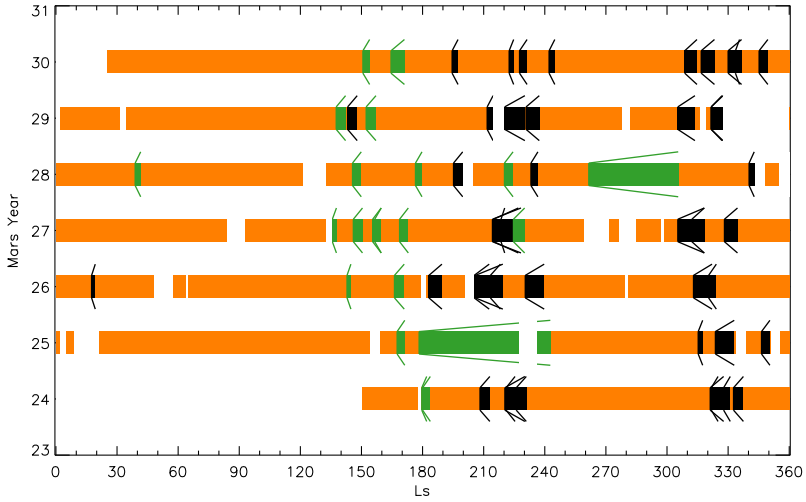

Fig. 2. Seasonal distribution of dust storm sequences observed in MGS MOC (Mars years 24–28) and MRO MARCI (Mars years 28–30) Mars Daily Global Maps (MDGM). Cap edge dust storms at high latitudes are neglected in this study unless they move to lower latitudes. Periods with missing MDGMs for each year are indicated by blanks. Periods with data but without any dust storm sequences are indicated by orange bars. Each identified sequence is indicated by a left bracket with the vertical line corresponding to the beginning and the other two sloped lines corresponding to the duration of the sequence. Each dust storm sequence is also indicated by a filled bar color-coded according to its origination hemisphere. Northern hemisphere originated sequences are in black and southern hemisphere originated sequences are in green. Note that a northern sequence can travel to the southern hemisphere and vice versa. (For interpretation of the references to color in this figure legend, the reader is referred to the web version of this article.)

storms, and the opposite seasons are characterized by sporadic large dust storms that vary from year to year. In their review of dust activity before the 1990s, Martin and Zurek (1993) found that large storms (storms larger than local events) only occurred during $L_s \sim 160$–$330°$. Our results show a somewhat wider seasonal window for non-local storms that adds the adjacent periods from $L_s \sim 130$–$160°$ and L_s 330–350°. This was also noticed in Cantor (2007). However, as will be shown later (Section 5), all of the largest dust storm sequences (with peak area $>1 \times 10^7$ km^2) are observed during $L_s \sim 130$–$320°$.

Fig. 2 shows that the northern sequences (black) are mainly concentrated in two seasonal windows – the northern fall ($L_s \sim 180$–$250°$) and the northern winter ($L_s \sim 305$–$350°$). There are typically several instances each year within each window. As will be shown later, the majority of these dust storms are related to frontal dust storms that later develop into flushing events (Wang et al., 2003, 2005; Wang, 2007). The northern sequence at $L_s \sim 143$–$148°$ in Mars year 29 was composed of daily dust storm in Chryse and showed limited eastward motion toward the Arabia border.

In addition to the two global dust storms, Fig. 2 shows that the southern sequences (green) are predominantly observed from mid to late southern winter ($L_s \sim 130$–$180°$). There were two non-global storm southern hemisphere sequences observed in mid-southern spring. One started from Hellas at $L_s \sim 224°$ in Mars year 27, and later merged with a sequence from Chryse (Section 5). The other also started from Hellas and traveled to Noachis during $L_s \sim 220$–$224°$ in Mars year 28.

Besides the difference in seasonality between the northern and southern sequences, there is also a difference in duration. Fig. 2 indicates that most southern sequences tend to be well separated in time and last for either only a few days (5 or more, by our definition) or several months (global dust storms). In comparison, the northern sequences sometimes form clusters and last either a few days or a few weeks. This will be discussed further in the next section. Although none of the northern sequences are observed to develop into global dust storm, some of them can develop into planet-encircling scale and lead to pronounced perturbations of the atmospheric structure and circulation (Wang et al., 2003; Liu et al., 2003; Smith, 2008).

Fig. 2 also shows some inter-annual variability of dust storm sequences. Global dust storms occurred in Mars years 25 and 28 at $L_s \sim 180°$ and 260°, respectively. The onset of the northern sequences following the global dust storms in Mars year 28 appeared to be delayed. Of the non-global dust storm years, Mars year 24 exhibited the longest hiatus between the northern fall storms and northern winter storms. In the northern fall of Mars years 28 and 30, there was a lack of weeks-long dust storm sequences.

3.2. L_s–area distribution

Fig. 3 shows the L_s versus area distribution of the dust storm sequences identified for all the Mars years examined. Again, a sequence is defined as lasting for $\geqslant 5$ days and influencing areas beyond their origin. On each day, there may be one or more discrete dust hazes or storms contributing to a sequence. We manually mark these dusty areas by judging the albedo contrast with the surroundings, the morphologies, the day-to-day variations and whether or not dust is thick enough to block the view of surface features. Each data point in Fig. 3 represents the total area of the contributing thick dust on that day. The data points for each sequence are connected. The area shown in Fig. 3 should be considered as a lower limit since it only includes the part of dust that appear to severely obscure the surface in MDGMs. The whole lifecycle of each sequence is plotted except for the global dust storms whose areas run off the top of the scale at $L_s \sim 180°$ and 260°, respectively. Of the 65 total dust storm sequences, 62 have peak areas $>1.6 \times 10^6$ km^2. The other 3 are only slightly below this limit, but their areas are still on the order of 10^6 km^2. Therefore, the vast majority of the dust storm sequences we study satisfy the definition of regional dust storm in Cantor (2007). All the sequences with peak areas $>5 \times 10^6$ cm^2 are observed during $L_s \sim 130$–$350°$, and those $>1 \times 10^7$ cm^2 are observed during $L_s \sim 130$–$320°$.

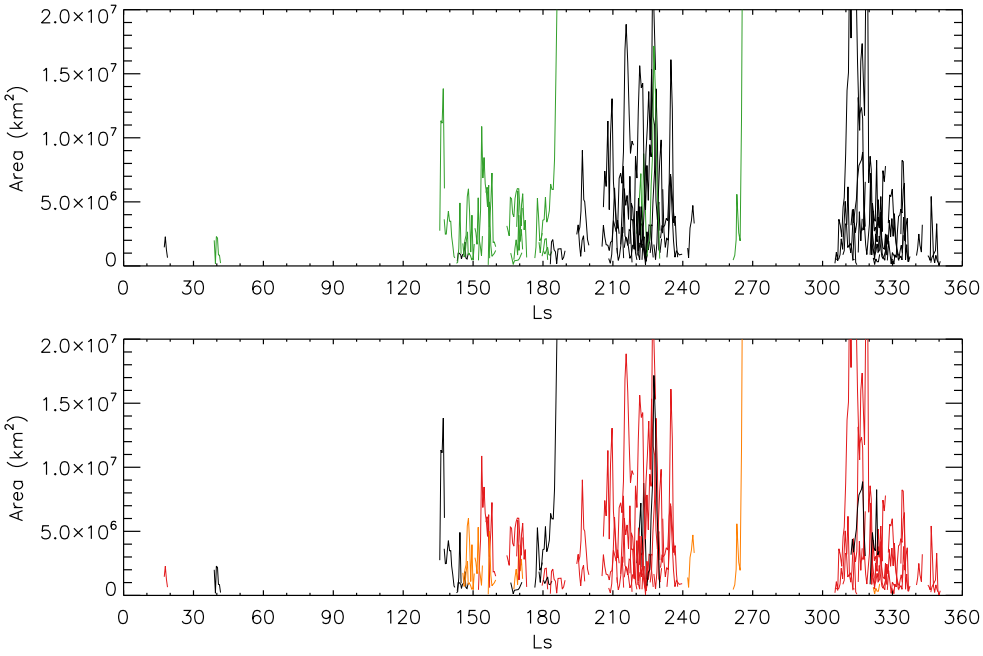

Fig. 3. Daily total areas of thick dust contributing to dust storm sequences as a function of L_s. All the sequences identified in MDGMs for Mars years 24–30 are plotted. Each sequence is connected with a line. In the top panel, northern sequences are colored black and southern sequences are colored green. In the bottom panel, sequences that involve frontal dust storms are colored red, sequences that do not are colored black and ambiguous cases are colored orange. (For interpretation of the references to color in this figure legend, the reader is referred to the web version of this article.)

In the top panel of Fig. 3, the northern sequences are colored black, and the southern sequences are colored green. Except for the global dust storms that explosively expand from the southern hemisphere, the northern sequences can be substantially larger than the southern sequences. Both the northern and southern sequences show preferred seasonal windows, as discussed in Section 3.1. Though some sequences stay within their origination hemispheres, others cross the equator at some points. In fact, large northern hemisphere-originating sequences often attain their maximum dust loading and extent in the southern hemisphere.

In the bottom panel of Fig. 3, the sequences associated with frontal dust storms are colored red, those exhibiting no frontal features are colored black, and ambiguous cases are colored orange. As long as there is at least one clearly identifiable frontal dust storm (with characteristic curvilinear shape) contributing to a sequence, regardless of where and when, then the sequence is colored red in this figure. Obviously, such a sequence can still have other types of dust lifting/storm morphology during its history and those other morphologies may or may not occur more often than frontal dust storms. By comparing the top and bottom panel, it can be inferred that most of the northern sequences are associated with frontal dust storms. The few larger ones are associated with flushing events (Cantor et al., 2001; Cantor, 2007; Wang, 2007; Hinson and Wang, 2010). These fronts are generally associated with the northern polar vortex and are believed to result from baroclinic instability, analogous to low-pressure frontal cyclones on the Earth (Wang et al., 2003). Curvilinear fronts could also develop along the cap edge due to the 'collision' of air masses off the cap with the surroundings (Toigo et al., 2002). A number of southern hemisphere sequences are also associated with frontal dust storms. Although within a given dust storm sequence, not all the component dust storms are frontal in nature (or remain frontal for the entire sequence), Fig. 3 suggests that frontal development is an important link in the evolution of most dust storm sequences. However, frontal dust storms are not involved in all dust storm sequences. The black lines in the bottom panel of Fig. 3 show a significant minority that exhibits no frontal/curvilinear structures.

Fig. 3 suggests that the sequences with larger peak areas are generally also the ones that last longer. However, some sequences that attain only moderate peak areas can also persist for extended time periods. This is better shown in the scatter plot of peak area versus duration measured in degrees of L_s (Fig. 4).

In the top panel of Fig. 4, a cluster analysis based on the peak area and duration divides the sequences into the following three groups. Note that other choices of clustering criteria and number of output groups will lead to different results.

- Group 1 contains the two global dust storms (which are off the scale of the plot, therefore not shown);
- Group 2 (red) contains 9 sequences that cluster around the regression line of $y = 7.5 \times 10^5 x + 1.2 \times 10^7$ and all the members have peak area $>1 \times 10^7$ km^2; Since the number of data points in this group is limited, the regression line is likely not robust, but the existing data suggest a positive correlation between the area and duration for the sequences in this group.
- Group 3 (blue) contains the rest, including the sequences with relatively short durations and small areas, as well as the 5 sequences that are >8° of L_s but $<1 \times 10^7$ km^2, which are in contrast to the members of Group 2.

In the bottom panel of Fig. 4, the northern sequences are colored black and the southern sequences are colored green. This panel shows that southern sequences that are not global storms are generally short-lived, with durations of less than 8° of L_s. There thus appears to be a lack of southern population with intermediate

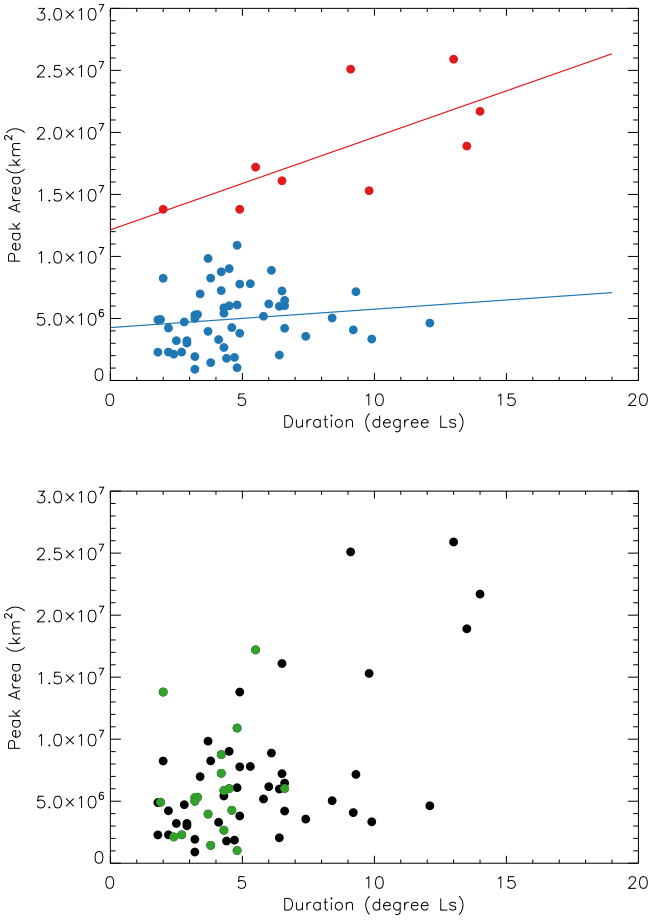

Fig. 4. The peak area versus duration of dust storm sequences. The 2001 and 2007 global dust storms are not included as they would be off the scale. The top panel shows the result of a cluster analysis and the regression line for each group. In the bottom panel, northern sequences are colored black and southern sequences are colored green. (For interpretation of the references to color in this figure legend, the reader is referred to the web version of this article.)

duration (southern storms are either relatively short lived or large global events). It can also be seen that the three largest non-global southern sequences with a peak area exceeding 1×10^7 km^2 last less than 6° of L_s. These sequences were observed in MDGMs during $L_s \sim 136$–138° in Mars year 27, $L_s \sim 224$–230° in Mars year 27 and $L_s \sim 152$–157° in Mars year 29.

In comparison, while northern sequences have not been observed to grow to global extent, the northern population includes sequences with intermediate as well as shorter durations. Among the northern sequences with intermediate durations of 7–15° of L_s (2 weeks–1 month), one set has peak area $>1 \times 10^7$ km^2. It is composed of sequences that involve cross-equatorial dust storms and that develop toward or into planet-encircling scale. They include one storm that traveled through Acidalia during $L_s \sim 220$–230° in Mars year 24 (Cantor et al., 2001; Wang et al., 2003), one that traveled through Utopia during $L_s \sim 205$–219° in Mars year 26, one through Acidalia during $L_s \sim 313$–322° in Mars year 26 (Cantor, 2007; Wang, 2007), one through Acidalia during $L_s \sim 214$–228° in Mars year 27, one through Acidalia during $L_s \sim 313$–322° in Mars year 27 (Hinson and Wang, 2010) and one through Acidalia during $L_s \sim 230$–237° in Mars year 29.

The remainder of the northern hemisphere, intermediate lifetime dust storm sequences have peak areas $<1 \times 10^7$ km^2. In some cases, dust storms were repeatedly observed for many days along a relatively short route, for example, in the Acidalia–Chryse channel. In other cases, dust storms progressed further each day following a

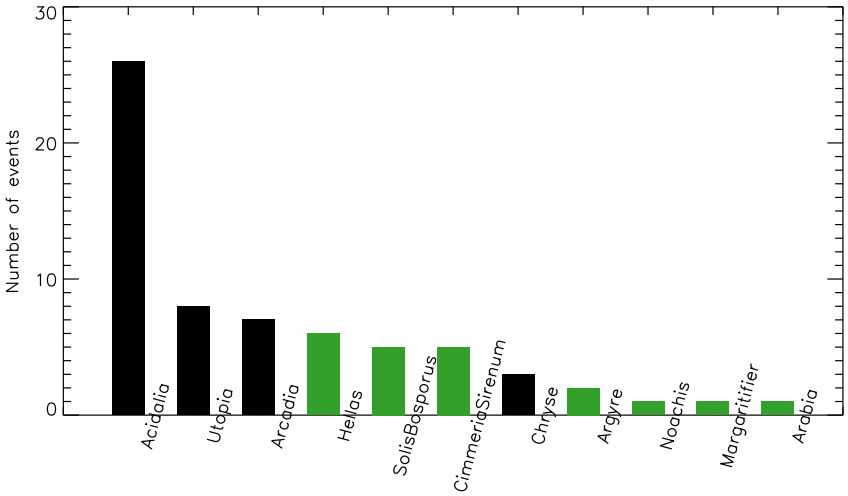

Fig. 5. Histogram of the origination regions of dust storm sequences observed in MGS and MRO MDGMs during Mars years 24–30. These regions are indicated in the MDGMs in Fig. 7.

long route, but only part of the long route was covered by thick dust on a particular day. However, in both types of cases, dust storms within the sequences were not able to initiate further growth. As a result, the dust storm sequences stayed much smaller than planet-encircling scale. The various development styles of dust storm sequences will be discussed in Section 5.

4. Origin locations and storm travel routes

4.1. Origination areas

Fig. 5 shows the histogram of the origination areas of the dust storm sequences. The northern sequences are colored black, and the southern sequences are colored green. Acidalia is the region where the most dust storm sequences originate, followed by Utopia, Arcadia and Hellas. Other regions include Solis/Bosporus, Cimmeria/Sirenum, Chryse, Argyre, Noachis, Margaritifier and the southern edge of Arabia. Most of these areas have previously been identified as frequent dust storm source regions (Martin and Zurek, 1993; Cantor et al., 2001; Cantor, 2007). The number of sequences from Acidalia is about three times of that from Utopia. Hinson et al. (2012) also found that Acidalia had much more frontal dust storm activity than other areas. Hinson and Wang (2010) suggested the following factors that affect the timing and location of regional frontal/flushing dust storms: (1) transitions among baroclinic wave modes, (2) storm zones and (3) stationary waves. While Acidalia is the most preferred region for the northern sequences, Hellas is the most preferred site for the southern sequences. In agreement with these observations, Mars GCM simulations suggest that the area north of Tharsis and upwind of Acidalia and the area in western and northern Hellas have strong surface stresses (Newman et al., 2002; Basu et al., 2006; Kahre et al., 2006; Toigo et al., 2012; Mulholland et al., 2013).

4.2. Routes

In Fig. 6, the observed routes traveled by dust storm sequences are plotted on a storm-free MDGM (60°S–60°N). This figure summarizes the variety of cases observed during Mars years 24–30 and indicates where dust storm sequences originate and where they go. The diagram is in the form of a graph (e.g. Hartsfeld and Ringel, 2003). The lines and arrows form unidirectional edges indicating the general routes. Note that the edges do not show the exact pathways of any specific sequence. Northern sequences are colored black and southern sequences are colored green. The dashed lines at the top and bottom indicate that circumpolar dust storms are neglected in this study. The dashed arrows near Hellas indicate the initial expansions of the global dust storms in Mars years 25 and 28. Subsequent development of global dust storms is not considered in this paper. The numbers in the graph indicate the number of sequences passing along the corresponding edge. A dust storm sequence can start from any edge, follow one or more subsequent edges, and terminate anywhere along the main route or branches. Consequently, the sum of numbers for the branches is different than the number for the main route.

Fig. 6 shows that the routes are distributed in areas where GCM simulations predict high surface wind stresses (Newman et al., 2002; Basu et al., 2006; Kahre et al., 2006; Toigo et al., 2012;

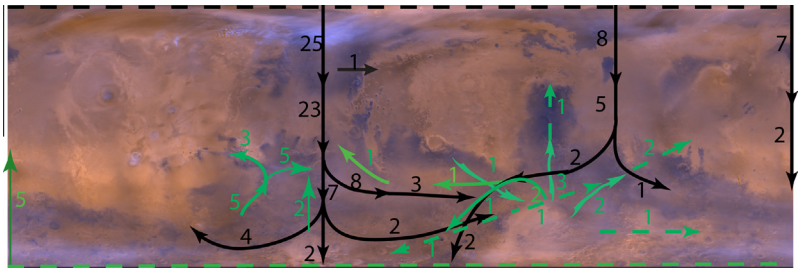

Fig. 6. Routes for dust storm sequences observed in MGS and MRO MDGMs during Mars years 24–30. Northern sequences are colored black. Southern sequences are colored green. Dashed lines at the top and bottom indicate that circumpolar dust storms are neglected in this study. Dashed arrows indicate the initial expansion of global dust storms. The number of sequences through each segment is indicated in the plot. (For interpretation of the references to color in this figure legend, the reader is referred to the web version of this article.)

Mulholland et al., 2013). The main east–west routes are in the southern hemisphere and the main north–south routes extend from the northern to the southern hemisphere. Although there are north–south routes from the southern hemisphere as well, they are generally shorter (except for those active during the global dust storms) and occur less frequently. Since planet-encircling dust storms imply longitudinal expansion to cover a latitudinal band, they are most likely to go through the southern hemisphere to achieve this status. However, many east–west routes are branches of the north–south routes and some north–south routes are observed to stretch over considerable latitudinal distances. Consequently, some nearly planet-encircling dust storms can be traced back to the northern hemisphere.

4.2.1. Northern sequences

Fig. 6 shows that the three main routes from the northern to the southern hemisphere are through Acidalia, Utopia and Arcadia. These sequences involve multiple frontal/flushing dust storms, as described in previous studies (Wang et al., 2005; Hinson and Wang, 2010). The majority of them dissipate in the northern hemisphere. However, a few impressive sequences go across the equator to the southern hemisphere where they dissipate or follow branches.

For the Acidalia sequences, one branch turns eastward in the southern low latitudes toward the corridor between Arabia and Noachis. An example can be found during $L_s \sim 220$–230° in Mars year 24 (Cantor et al., 2001; Wang et al., 2003). The other branch continues further south toward Argyre and beyond, turns toward Hellas and/or Solis. An example can be found during $L_s \sim 313$–322° in Mars year 26 (Cantor, 2007; Wang, 2007).

A few Utopia sequences continued across the topographic dichotomy. One sequence ($L_s \sim 233$–236° in Mars year 28) turned slightly eastward toward Hesperia/Cimmeria. Two sequences ($L_s \sim 206$–219° in Mars year 26 and $L_s \sim 305$–314° in Mars year 29) turned westward and went around the area north of Hellas toward Noachis and beyond. Both routes are consistent with the surface wind directions simulated by GCM for the corresponding seasons (Toigo et al., 2012).

For the Acidalia and Utopia sequences that travel very long distances from the north to the south, while the early stage dust lifting activity is clearly in the northern hemisphere, later on in the storm evolution, the major dust loading and lifting centers shift to the southern hemisphere. The ones that exhibit longitudinal expansion in the southern hemisphere can grow into planet-encircling dust storms (Cantor et al., 2001; Cantor, 2007; Wang et al., 2003; Wang, 2007). The relationship of a briefly observed Acidalia/Chryse storm to the origin of the 2007 global storm is highly ambiguous (see Section 5.3).

The longest Arcadia sequence observed so far was during $L_s \sim 226$–231° in Mars year 24 (Fig. 8). It traveled southward across the equator to Sirenum/Cimmeria. Although the flushing dust storms in the Arcadia sequences appeared as impressive as those in Acidalia or Utopia sequences (Wang et al., 2005), they are observed less frequently. Within our data set, the Arcadia sequence usually covers shorter latitudinal range and exhibits no or little longitudinal expansion.

4.2.2. Southern sequences

Hellas is the most important origination area of the southern sequences observed so far. Routes go in many directions toward Hesperia, Elysium, Syrtis, Noachis and the south polar cap. The 2001 global dust storm originated from the western and northern slopes of Hellas. It exhibited rapid eastward expansion to Hesperia and northward expansion to Syrtis at the beginning, and later involved a second major dust lifting center in the Syria/Solis area later on (Smith et al., 2002; Strausberg et al., 2005; Cantor, 2007). For the 2007 global dust storm, the first major dust lifting was in the Noachis/West Hellas area, though there was a preceding (and ambiguously related) sequence from Chryse (Section 5).

The region enclosed by Syria, Argyre and Valles Marineris (labeled as Solis/Bosporus in Fig. 5) is also a common origination area for southern sequences, so is the Cimmeria/Sirenum region. The corresponding sequences generally move northward toward the equator. Some Solis/Bosporus sequences appear to travel along Valles Marineris. Martin and Zurek (1993) pointed out that the Syria/Solis area was an important dust source region for global dust storms, but not for local dust storms. Consistent with their results, our observations show that the Syria/Solis area seldom had local dust storms, but was active after the initiation of both 2001 and 2007 global dust storms and was also involved in several other dust storm sequences. This behavior suggests that dust lifting in the area may require enhancement of the circulation resulting from the collective effect of other dust lifting centers in order to become activated.

5. Development styles

5.1. Classification

The most common development style observed for dust storm sequences is the daily repetition of dust storms traveling along the same route, keeping the region dusty for 5 sols or more. We will simply call this style of development "consecutive dust storms". This type can be seen in Fig. 7a–e where Days 10–14 of a dust storm sequence during $L_s \sim 214$–228° in Mars year 27 is shown. On each day, there are one or more dust storms within the Acidalia–Chryse channel. This consecutive dust storm sequence appears to be related to frequent frontal initiation (or "pumping" of the storm by frontal systems) in the high northern latitudes. Similar frontal/flushing dust storms are observed in the area daily for the first 3 weeks or so of the sequence. If the generation of the flushing events is associated with coherent timing of the low-pressure weather systems having favorable phase of the thermal tide (Wang et al., 2003), then this extended time period probably represents an extended time period of near-phase locking of the systems.

Another development style is through sequential activation of one segment of a route after another as the whole sequence advances forward. We will call these "sequential activation dust storms". Example images can be found in Figs. 19 and 20 of Cantor (2007) and Figs. 2 and 3 of Wang (2007). These examples show the development of dust storm sequences originating in Utopia–Isidis during $L_s \sim 210$–220° and in Acidalia–Chryse during $L_s \sim 310$–320° in Mars year 26. In each case, the dust activity center progressed further each day along the route. As a new segment become dusty, dust in the previous segment dissipated. The Acidalia sub-sequence shown in Fig. 7 can be considered to belong to this category since dust activity shifted from the northern to the southern hemisphere with time.

A third development style is through the merging of dust from two or more initially separate sequences to create a contiguous dust cover. We will call these "merging dust storms". This appeared to be a very effective way of making larger dust storms, including the two global storms. The 2001 global storm resulted from the merger of dust from storms (or alternatively, lifting centers) originating near Hellas and Syria-Solis area (and potentially also in the northern high latitudes) (Strausberg et al., 2005; Cantor, 2007). Fig. 7 shows an example for this type, too. During the course of the Acidalia sequence, another sequence started from northern Hellas (Fig. 7f) and traveled toward Noachis (Fig. 7g). In the

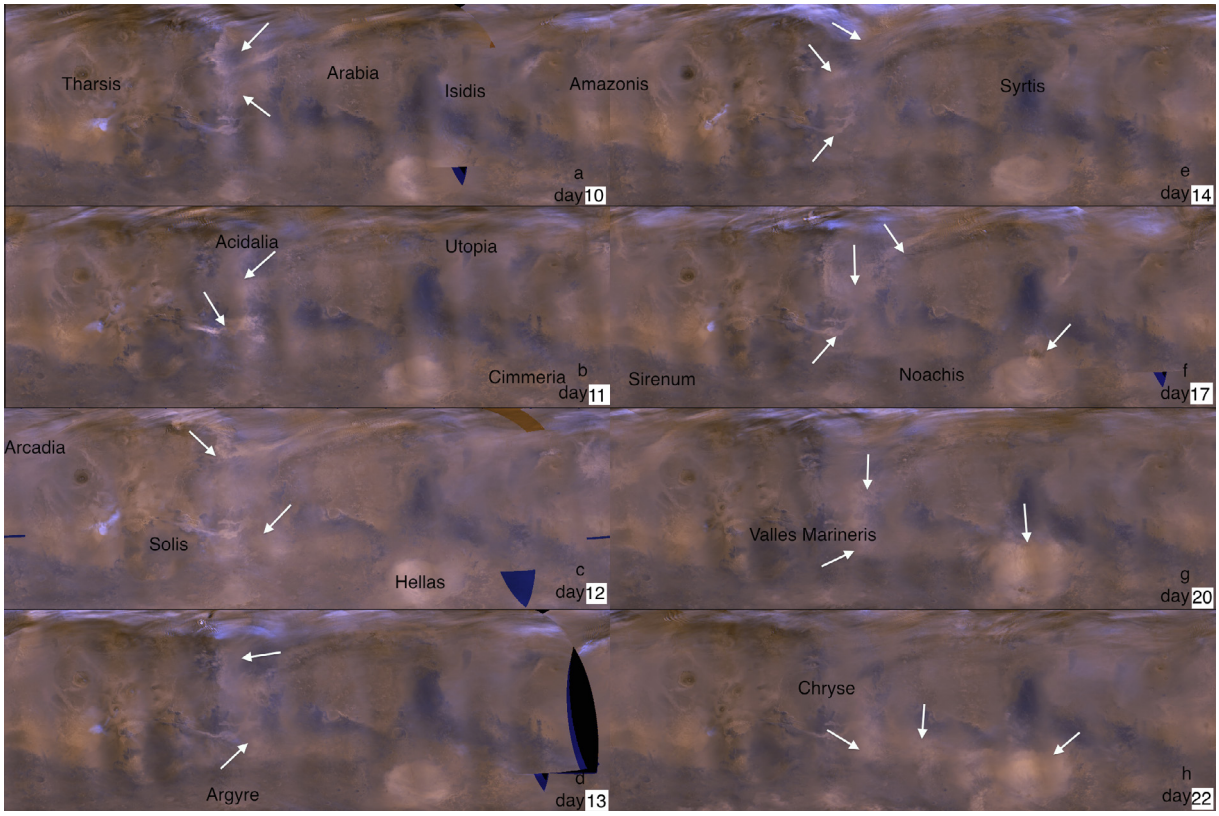

Fig. 7. Example MGS MDGMs (60°S–60°N, in simple cylindrical projection) for the development of the dust storm sequence during $L_s \sim 214–228°$ in Mars year 27. Member dust storms are indicated by white arrows. (a) Day 10, (b) Day 11, (c) Day 12, (d) Day 13, (e) Day 14, (f) Day 17, (g) Day 20 and (h) Day 22.

meanwhile, the Acidalia sequence turned toward the corridor between Noachis and Arabia, and merged with the Hellas sequence.

There can be different combinations of these development styles for a sequence. In another word, a dust storm sequence can exhibit different development styles at different stages. This is clearly the case in the example shown in Fig. 7. The overall development is through "merging" of the Acidalia and Hellas sub-sequences. The Acidalia sub-sequence contributing to the total storm sequence can be further classified as "sequential activation" since the dust activity moved from the northern hemisphere to the southern hemisphere, but the first ~2/3 of the Acidalia sub-sequence developed through "consecutive dust storms" in the Acidalia–Chryse channel. The Hellas sub-sequence also developed through "consecutive dust storms" in the Hellas–Noachis area.

5.2. Overlap

As mentioned earlier, dust storm sequences can overlap in time. For example, during $L_s \sim 220–230°$ in Mars year 24, a dust storm sequence developed from Acidalia and headed toward Argyre and the corridor between Arabia and Noachis (Cantor et al., 2001; Liu et al., 2003). During the course of this sequence, two other sequences were observed – one from Utopia to Elysium during $L_s \sim 221–225°$, and the other from Arcadia to Cimmeria/Sirenum during $L_s \sim 226–231°$. The L_s versus area plot of the three sequences observed in MDGM is shown in Fig. 8a. The day-to-day variability shown by the curves is probably not statistically significant since there are cases where dust storms gradually merge to the background, making it difficult to decide on the border. However, the relative size of the sequences is robust. The Acidalia sequence (shown in red) had the longest duration and the largest peak area. The Utopia sequence (shown in green) was much smaller and shorter. The Arcadia sequence (shown in purple) achieved nearly the same peak area as that of the Acidalia sequence, but lasted only half as long.

Fig. 8b shows the areas affected by the Acidalia (red), Utopia (green) and Arcadia (purple) sequences as judged by visual inspection of MDGMs. We identify dusty areas on each day for each sequence. As long as a pixel is considered dusty at some point during the observational period of $L_s \sim 220–230°$, it is highlighted in the figure. In another word, the highlighted areas were apparently covered by dust on one or more days during $L_s \sim 220–230°$. Most of the areas in the northern plains were involved. All three sequences contributed dust to the low latitudes. The Acidalia and Arcadia sequences penetrated to the southern mid-latitudes.

Liu et al. (2003) tracked the dust activity described above using optical depth maps derived from MGS TES data for every 2° of L_s during $L_s \sim 205–245°$ in Mars year 24. Their results showed that a nearly continuous dust band formed at the southern low latitudes after $L_s \sim 231°$. Although TES data did not allow some of the details of the dust storm structures to be observed due to their limited spatial resolution and coverage as compared with MDGMs (Wang et al., 2013), they were able to describe the overall development history of this long lasting event.

In Fig. 8c, we have plotted the maximum TES dust optical depth for each $4° \times 5°$ grid box during the $L_s \sim 220–230°$ period of Mars year 24. There are typically about 300 data points in each grid box. The low topographic channels from Acidalia, Utopia and Arcadia show high dust amount, as well as the Corridor between Arabia and Noachis in the southern low latitudes. The dust optical depth in the plot is not normalized to the same pressure level. However, a comparison with similar plots for dust storm free periods (not shown) clearly indicates that the high optical depths result from the three overlapping dust storm sequences described previously. The optical depths shown in Fig. 8c also include contributions from sporadic dust storms and dust hazes whose effect accumulates

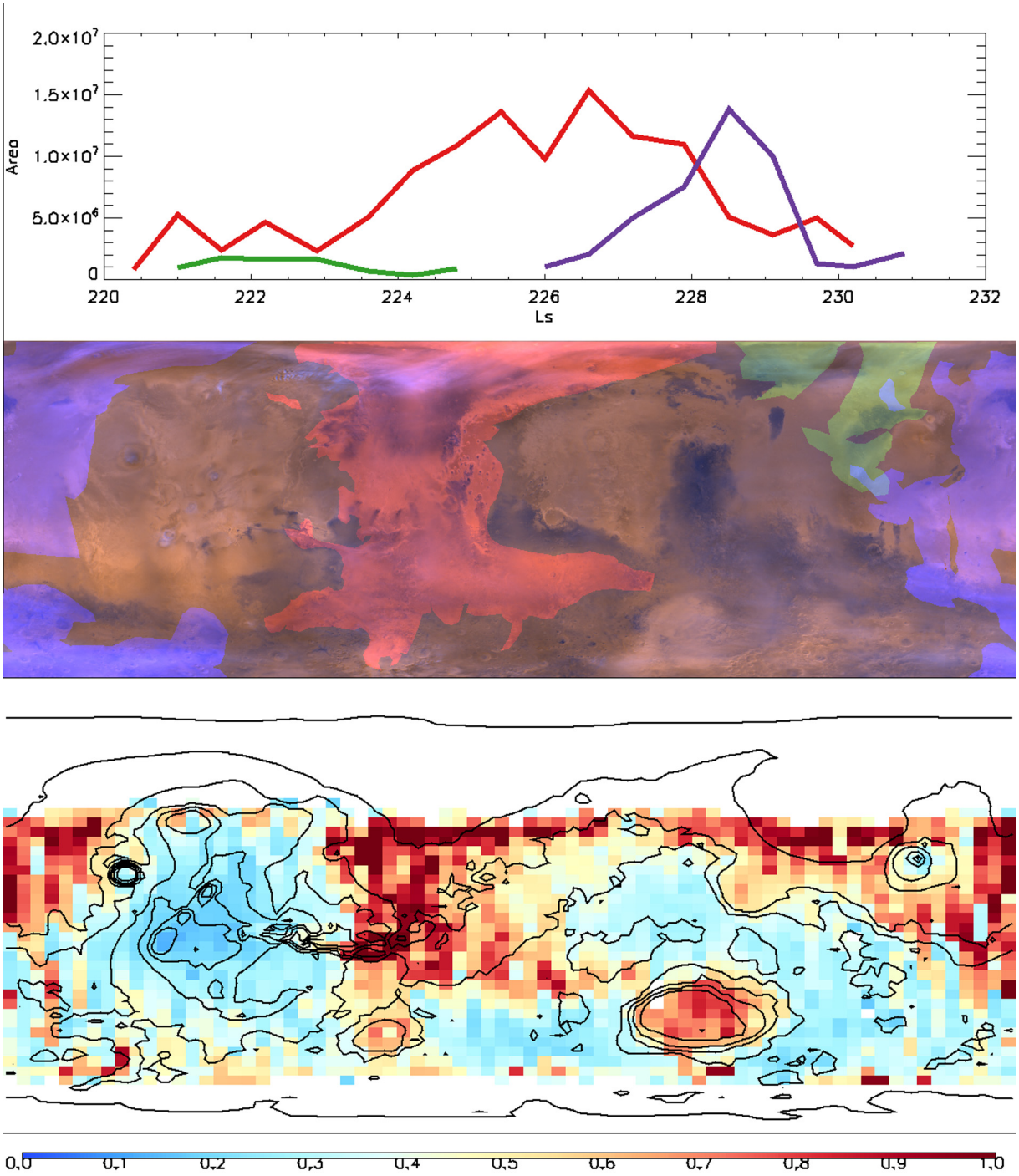

Fig. 8. (a) L_s versus area plot of the dust storm sequences observed during $L_s \sim 220$–$230°$ in Mars year 24. The Acidalia sequence is shown in red, Utopia sequence in green and Arcadia sequence in purple. (b) The area in MDGM (60°S–60°N) that is apparently affected by the dust in the Acidalia (red), Utopia (green) and Arcadia (purple) sequence. (c) The maximum MGS TES dust optical depth for each $4° \times 5°$ grid box during $L_s \sim 220$–$230°$ in Mars year 24. (For interpretation of the references to color in this figure legend, the reader is referred to the web version of this article.)

during the analysis window. The MDGM images indicate that these events are mostly near the edge of the southern polar cap and Hellas, distinguishing them from the dust storm sequences.

To investigate when dust storm sequences overlap during our observational period, in Fig. 9 we have indicated dust storm sequences with brackets on the L_s versus latitude map of the zonal mean atmospheric temperatures. The temperature data are from the 2 AM TES temperatures at 64.3 Pa (Mars years 24–26, Smith, 2004), the 5 PM THEMIS temperatures at ~50 Pa (Mars years 27–28, Smith, 2009) and the 3 AM MCS temperatures at 64.3 Pa (Mars years 29–30, Kleinboehl et al., 2009). Note the differences in local time and pressure level. The vertical edge of a bracket corresponds to the first day of a sequence. The other two edges extend to the last day of the sequence (except for global dust storms). We have marked the sequences larger than 10^7 km^2 with '×'s on the corresponding brackets.

Overlapped sequences are represented by overlapped brackets in Fig. 9. It can be seen that overlap in our observational period

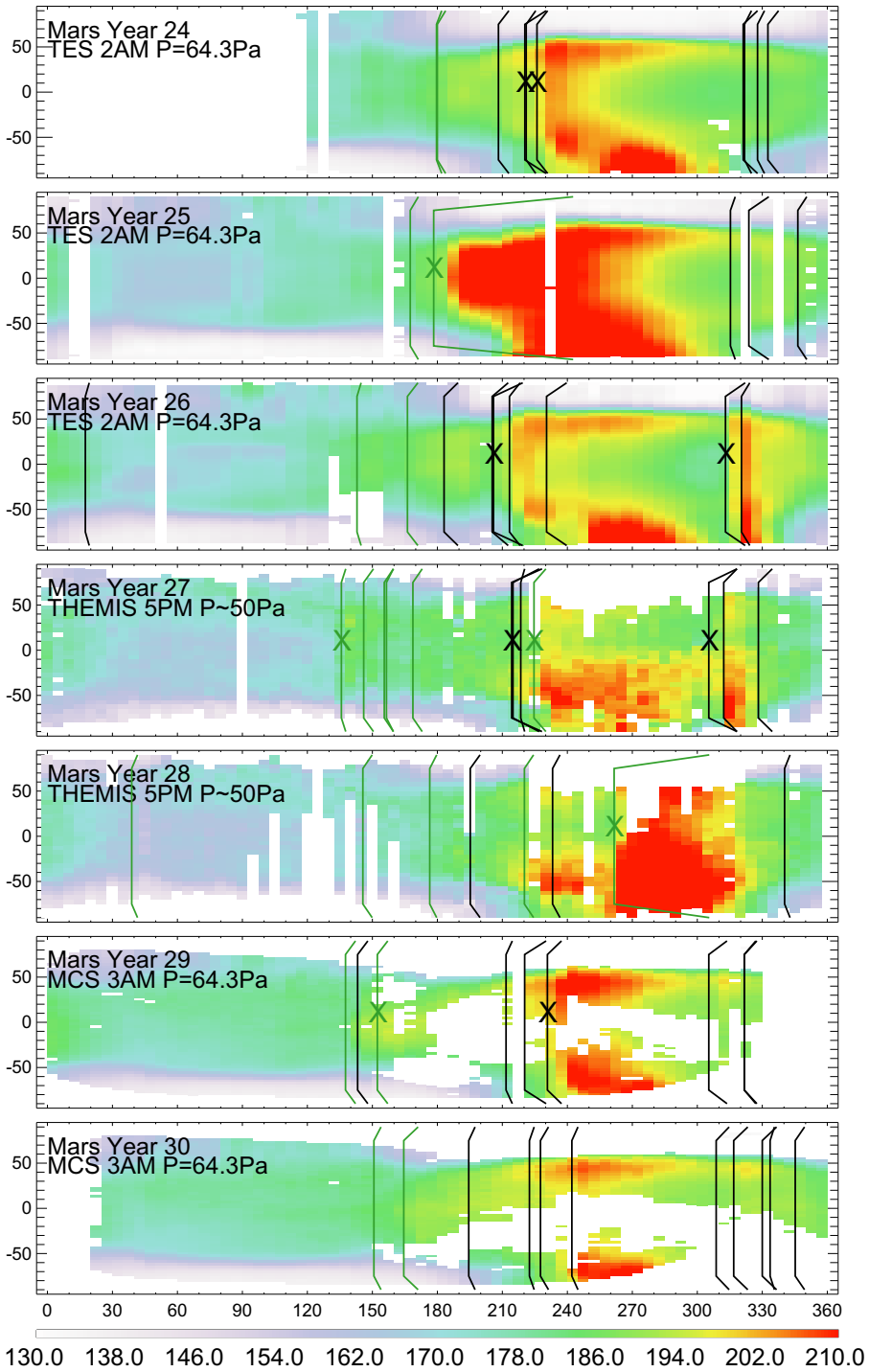

Fig. 9. Filled contours show the L_s – latitude distribution of the zonal mean atmospheric temperate (K) at 64.3 Pa derived from MGS TES 2 AM data (Mars years 24–26), at ~50 Pa derived from Mars Odyssey THEMIS 5 PM data (Mars years 27–28) and at 64.3 Pa derived from MRO MCS 3 AM data (Mars years 29–30). Missing temperature data are left blank. The left brackets indicate the starting L_s and duration of dust storm sequences identified in MGS MOC or MRO MARCI MDGMs. Northern sequences are colored black and southern sequences are colored green. Sequences with peak areas $>10^7$ km^2 are indicated by '×'s. (For interpretation of the references to color in this figure legend, the reader is referred to the web version of this article.)

is mainly observed during $L_s \sim 200$–$240°$ and $L_s \sim 300$–$340°$. There are 8 cases of overlap during these two seasonal windows, six of them involve sequences with peak area $>10^7$ km^2, indicating that overlapped dust storm sequences are good candidates for expansion to larger scale. As mentioned in Section 3.2, we did not attempt to map separate dust storm sequence overlapping with the global dust storms due to concern over the degree to which the global events would have fundamentally changed the large-scale circulation. Had we done so, we count 10 cases of overlap during the $L_s \sim 175$–$340°$ window, about 80% of them with peak area $>10^7$ km^2. There is only one instance of an overlap outside this time period. It was observed during $L_s \sim 155$–$160°$ in Mars year 27 when one sequence traveled from Cimmeria/Sirenum to Amazonis and the other from Argyre to Valles Marineris. They were relatively

small and located far away from one another. So, not every temporal overlap necessarily led to a large dust storm. Other examples can be found in the post-solstice period of Mars years 24 and 30.

5.3. Large sequences

The available data in Fig. 9 suggests that sequences with peak area $>10^7$ km^2 in the northern fall and winter are associated with pronounced atmospheric temperature increases. In the early stage of the 2001 global dust storm in Mars year 25, the temperature increase appeared to be mainly in the low latitudes. For all other cases during these two seasons, including the middle and late stages of the 2001 global dust storm, the temperature field exhibited a bimodal distribution with one maximum at the southern mid/high latitudes and the other at the northern mid/high latitudes. Similar signatures in mid-level air temperatures following major dust storms had been reported in many previous studies and attributed to dust radiative heating in the south and dynamical heating in the north (Liu et al., 2003; Smith, 2004; Martin and Zurek, 1993). The MCS data show a bimodal temperature distribution in the fall of Mars year 30, though the dust storm sequences observed in the northern fall and winter seasons are all $<10^7$ km^2. However, the peak area of the largest storm of that year (during $L_s \sim 227$–$231°$ that year) was just short of 10^7 km^2. Considering the uncertainty of the area measurements, this sequence may be considered to be large. The sequence during $L_s \sim 242$–$249°$ in that year covered a very long latitudinal distance from Acidalia to Argyre. However, its area on each day remained relatively small as the sequence developed in a "sequential activation" fashion.

There were two southern sequences with peak area $>10^7$ km^2 observed in the northern spring and summer, although we measured both to be just slightly above the threshold. The THEMIS 5 PM atmospheric temperatures at ~50 Pa showed an increase above background values following the development of the dust storm sequence from Arabia to Hellas during $L_s \sim 136$–$138°$ in Mars year 27. The MCS 3 AM temperatures at 64.3 Pa showed an increase at low latitudes as compared with those of the next year after the sequence from Cimmeria/Sirenum to Amazonis during $L_s \sim 152$–$157°$ in Mars year 29.

5.4. Initiation of the 2007 global dust storm

Previous image observations suggest that global dust storms originate in the southern hemisphere during the southern spring and summer dust storm season (Martin and Zurek, 1993; Strausberg et al., 2005; Cantor, 2007). Two global dust storms occurred during our observation period – the 2001 global dust storm at $L_s \sim 180°$ in Mars year 25 and the 2007 global dust storm at $L_s \sim 260°$ in Mars year 28. While the 2001 global storm was unambiguously triggered in the mid-southern latitudes, the origin of the 2007 storm was less obvious. The major growth of the 2007 storm was at southern mid-latitudes between Hellas and Noachis. However, a confined ("flushing") dust storm was observed moving southwards from Chryse to Margaritifer Terra prior to the onset of subsequent major dust lifting. This raises the possibility that the Chryse storm in some way triggered or merged with the southern mid-latitude dust storm.

Fig. 10 shows ten consecutive MARCI MDGM (90°S–90°N) near the beginning of the 2007 global dust storm ($L_s \sim 261$–$267°$). Note that each MDGM is composed of 13 sets of consecutive global image swaths spaced about 2 h apart and that the 1st swath of each MDGM is the same as the 13th swath of the previous MDGM. The figure shows that during the first 3 days of the sequence, a dust storm from Chryse traveled southward to the east of Valles Marineris. It is possible that the Chryse storm arrived in the Noachis region by Day 5. However, the image coverage makes it hard to be certain, as will be explained next. The dust associated with this flushing event appears to have dissipated after Day 5 when new dust lifting centers near Noachis took over.

The Chryse dust storm occurred immediately prior to the onset of the 2007 global dust storm and it is tempting to associate this flushing event with the origin of the global storm. Ambiguity in this association, however, arises from the nature of the data coverage. The Chryse flushing event is captured in image Swath 13 of Day 2 which is the same as Swath 1 of Day 3. As such, there is no new information on the event in Day 3. However, Swath 13 of Day 3 shows a dust cloud about 2000 km to the southeast (in the Noachis region). The connection between these events is ambiguous. If the dust clouds were the same event caught at different times (about a sol apart), and transport was the dominant processes in the continuity of the cloud (rather than new lifting), it would require an advection speed of about 25 m/s. Such speeds are not beyond the range of possibility, but it would require the average wind to be at this high speed for the full day. Considering the wind direction rotation associated with thermal tides, much higher instantaneous winds would be required if they were from the same dust cloud (e.g., Wilson and Hamilton, 1996).

There appear to be two dust centers on Day 4, although the Noachis dust cloud is in Swath 1, which is again a repeat of Swath 13 of Day 3. The other dust cloud is located to the west of the Noachis dust cloud. However, the seam between the swaths prevents a clean interpretation. This dust cloud could be a part of the Noachis storm, a continuation of the flushing storm on the previous day, a new flushing dust storm or a new dust lifting center. It should be noted that on Day 5, the Noachis dust cloud remained roughly at the same area as that on the previous day. This seems to be at odds with a rapid advection of a flushing event to Noachis during Day 3.

The global map swaths have greatly improved our observations of martian dust storms. However, some critical information is unfortunately lost due to the fixed local time coverage from polar orbits. Continuous monitoring from a geostationary orbit would eliminate the guessing, and further improve our understanding of the martian dust cycle.

While it is uncertain to somewhat unlikely that the dust cloud from the Chryse flushing event is the same as the one that appears in Noachis on Day 3, the images cannot tell us whether a dynamical coupling existed between these regions. It would be interesting to examine how the heating resulting from the Chryse storm modified the circulation and whether this was in part responsible for dust lifting in Noachis that directly began the 2007 global dust storm.

It is particularly interesting to note that during the $L_s \sim 260$–$270°$ period for Mars years 24–30, we have only identified one Chryse dust storm sequence: the event discussed here that directly preceded the 2007 global dust storm (in Mars year 28). Indeed, it should be noted that in the Oxford Mars GCM, flushing dust storms were a common feature (Newman et al., 2002) and that they could trigger global dust storms (Mulholland et al., 2013), however, it is unclear with such small-number-statistics whether the correlation of the Chryse storm with the 2007 global dust storm is coincidence or causation, and the putative mechanism of any linkage remains to be elucidated beyond the speculative "enhancement" of the circulation.

The remainder of the 2007 global dust storm initiation played out directly from the Noachis dust storm. The MDGM sequence shows the lifting in Noachis to strengthen over the next 3 sols with very little lateral motion (Fig. 10). A threshold appears to have been dramatically crossed between Day 6 and 7, as the storm explosively grew during Day 7. Multiple secondary dust lifting centers appear to have become involved as early as Day 8 or 9 in the MDGM sequence. By the 10th day, the storm is well on its way toward planet-encircling scale. During Days 7–10, the dust rapidly

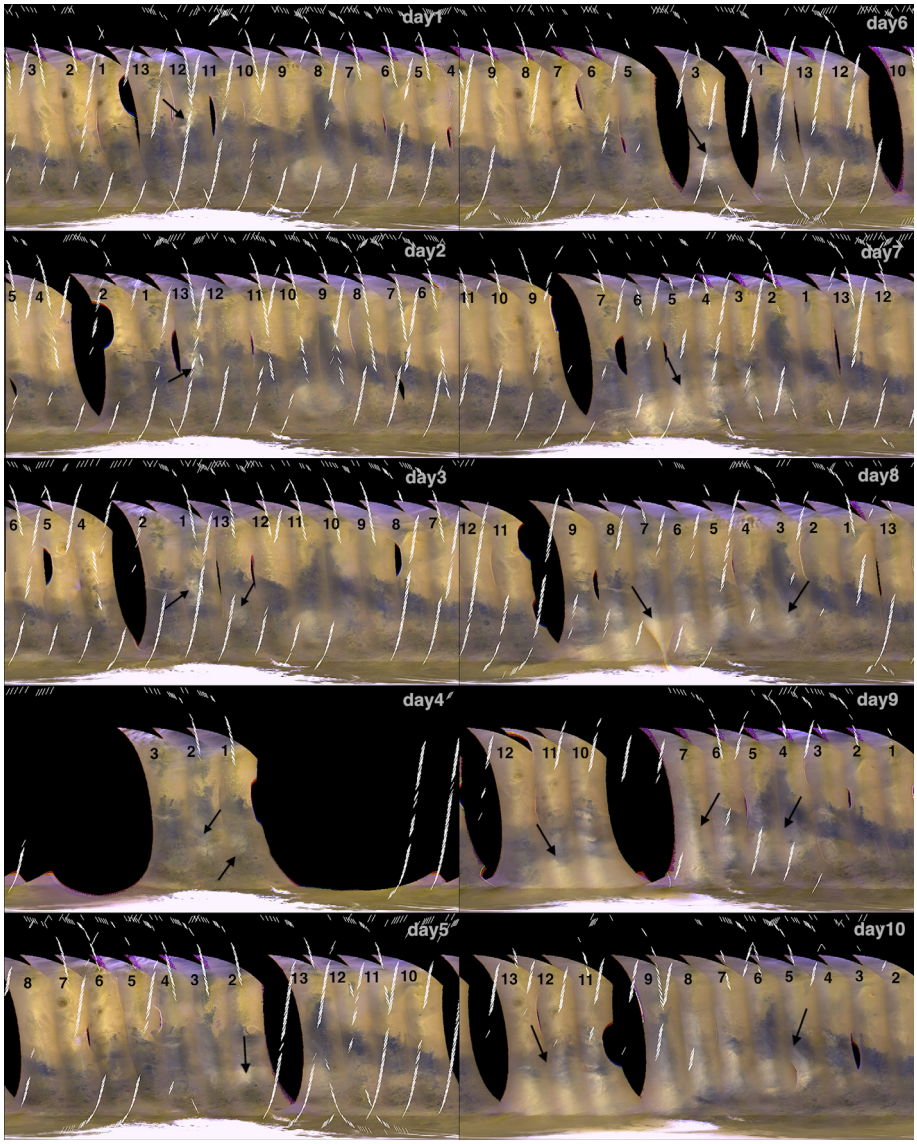

Fig. 10. MRO MARCI MDGMs near the beginning ($L_s \sim 261$–$267°$) of the 2007 global dust storm in Mars year 28. Each image shows the area between 90°S and 90°N in simple cylindrical projection. Images #1 to #13 indicated in each panel are sequentially taken by MARCI and pieced together in each MDGM. Consecutive MDGMs overlap by one orbit (image #13 of the previous day is the same as image #1 of the present day). Missing data or data in error are shown in black. The sampling distribution of the MRO MCS dust optical depth at 3 AM is shown by '/' (oriented northeast–southwest) and that at 3 PM is shown by '\' (oriented northwest–southeast). The black arrows indicate dust storms.

expanded along a primarily east–west axis, but with a notable northeast–southwest tilt, with expansion mainly to the south south west (SSW) and to a lesser extent to the north north east (NNE).

Fig. 11 shows the latitude versus height (km) cross-sections of the vertical distribution of MCS dust opacity (Kleinboehl et al., 2009) for the 10 days shown in Fig. 10. The spatial distribution of nighttime sampling is shown by '/' (oriented northeast–southwest) and that of daytime sampling is shown by '\' (oriented northwest–southeast) in Fig. 10. Since the nighttime sampling has much better coverage, especially for the low latitudes, we have plotted the 3 AM MCS data in Fig. 11. The MARCI images were taken at 3 PM, therefore, there is half a day offset between Figs. 10 and 11. Most of the tracks that cut across dust storms in Fig. 10 are for the nighttime, i.e., they do not coincide with the dust storms in images, but are within a day of their occurrences.

In Fig. 11, the 3 AM MCS dust optical depths are binned onto 4° latitude × 30° longitude grid, and interpolated onto fixed heights above local surface from the 105 fixed pressure levels of the MCS retrieval. The zonal maxima are extracted and their log values plotted for the lowest 50 km. We use the zonal maximum to indicate the height of dust penetration for a zonal band. Due to the sparse coverage of MCS dust optical depth at low latitudes (Fig. 10), the maximum is usually derived from only 2–6 orbits for the day. The MCS dust retrievals typically have errors within 20% and are difficult under high dust opacity conditions (Kleinboehl et al., 2009). Therefore, the plotted quantity may contain substantial error and the details of the panels should not be over interpreted. Nevertheless, the dust top after Day 6 is consistently higher than that before Day 6, suggesting that the imaged dust clouds are consistent with an overall deepening of dust mixing. Days 6–9 corresponded to the rapid horizontal expansion towards planet-encircling scale (Fig. 10). The comparison of the MCS cross sections with the MARCI MDGMs indicates that there was rapid dust expansion to high altitude after lifting began in Noachis region.

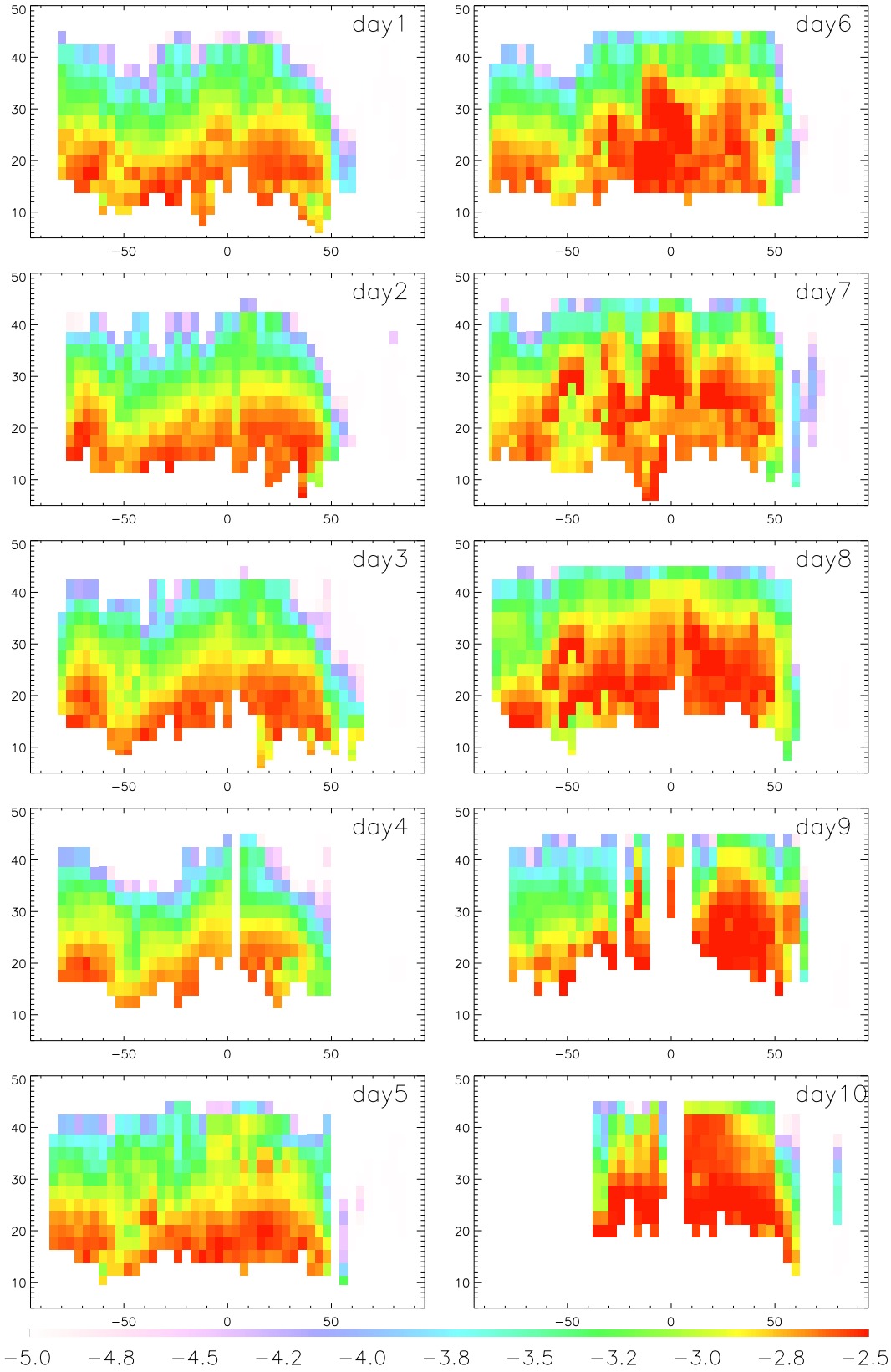

Fig. 11. Log10 of the zonal maximum of the 3 AM MCS dust optical depth for the 10 days shown in Fig. 10.

6. Summary

We have presented dust storm sequences observed in MGS MOC and MRO MARCI Mars Daily Global Maps during Mars years 24–30 to study the origin, evolution and trajectory of large dust storms on Mars. These sequences last for 5 or more sols, travel long distances and affect multiple regions. Each sequence is composed of daily dust storms that collectively show a continuous develop-

ment history. To simplify, we have neglected dust storms in the polar regions and dust storm sequences that may have developed during global dust storms.

We have visually inspected each MDGM and subjectively identified dust storm sequences. For each sequence, we have recorded the L_s at the beginning and end, the origination region, the area occupied by optically thick dust on each sol, the route traveled and whether or not frontal dust storms are involved.

Our results show that these dust storm sequences are most frequently observed during the $L_s \sim 130$–350° period, but that a single definition of a "dust storm season" combines several different families of dust storm types with different seasonal behavior. Specifically, sequences originating from the northern hemisphere (northern sequences) are mainly concentrated in two seasonal windows during the northern fall ($L_s \sim 180$–250°) and winter ($L_s \sim 305$–350°). All but two sequences originating from the southern hemisphere (southern sequences) are observed during $L_s \sim 135$–245° and most of them are concentrated in the period of $L_s \sim 135$–185°. The interval between $L_s \sim 250$–305°, which had typically been considered to be in the middle of the "dust storm season" exhibits only one sequence during the study period: the 2007 global storm in Mars year 28. The only other global storm in this study is the 2001 global storm (in Mars year 25).

None of the northern sequences are observed to develop into global scale, but some of them develop into the next biggest scale, with peak area $>1 \times 10^7$ km^2 and duration on the order of several weeks. In comparison, although the explosive growth of the 2001 and 2007 global dust storm occur in the southern hemisphere, there appear to be a lack of southern sequences with lifetime of a few weeks. As a result, northern sequences dominate the dust storm area fraction in non-global dust storm years.

The most preferred origination region is Acidalia, followed by Utopia, Arcadia and Hellas. For non-global dust storms, the main east–west routes are in the southern hemisphere, but the main north–south routes are from the northern to the southern hemisphere. The routes from Acidalia and Utopia show branches in the southern low/mid-latitudes. They are adopted by a few impressive cross-equatorial northern sequences.

Dust storm sequences develop through various combinations of development styles – "consecutive dust storms", "sequential activation" or "merging". Dust storm sequences may overlap in time. During our observational period, about 80% of the overlapped sequences in the northern fall and winter season involve sequences with peak area $>1 \times 10^7$ km^2 and are associated with pronounced increase in mid-level atmospheric temperatures. In mid/late northern summer, there are two southern sequences with peak area $>1 \times 10^7$ km^2, but they are smaller than those during northern fall and winter.

The origin of the 2007 global dust storm is somewhat complicated by the development of a northern-to-southern hemisphere flushing event from Chryse immediately prior to major dust lifting and explosive growth from Noachis. It is unclear whether the Chryse storm traveled to Noachis due to image coverage. Further study is needed to elucidate whether there is a dynamical link between the Chryse and Noachis dust storm. It is clear from the MDGMs that the development of the 2007 global dust storm from sub-regional to planet-encircling scale occurred in the southern hemisphere. The expansion to high altitudes occurred rapidly after lifting had occurred in Noachis. On this basis, we have categorized the 2007 global dust storm as a southern hemisphere sequence.

MGS MOC and MRO MARCI daily global map provide us an opportunity to derive the statistics and explore the complexity of the dust storm sequences that have the potential to grow bigger. Continued long-term spacecraft observation is invaluable for better understanding of the martian dust cycle.

Acknowledgments

This paper is supported by NASA's Mars Data Analysis program. We thank Michael D. Smith for providing the gridded TES and THEMIS data that are used in Fig. 9. We thank Michael D. Smith and Alexey Pankine for their reviews.

Appendix A. Supplementary material

Supplementary data associated with this article can be found, in the online version, at http://dx.doi.org/10.1016/j.icarus.2013.10.033.

References

Basu, S., Wilson, R.J., Richardson, M.I., Ingersoll, A.P., 2006. Simulation of spontaneous and variable global dust storms with the GFDL Mars GCM. J. Geophys. Res. 111, E09004. http://dx.doi.org/10.1029/2005JE002660.

Bell III, J.F. et al., 2009. Mars Reconnaissance Orbiter Mars Color Imager (MARCI): Instrument description, calibration, and performance. J. Geophys. Res. 114, E8. http://dx.doi.org/10.1029/2008JE003315.

Cantor, B.A., 2007. MOC observations of the 2001 Mars planet-encircling dust storm. Icarus 186, 60–96. http://dx.doi.org/10.1016/j.icarus.2006.08.019.

Cantor, B.A., James, P.B., Caplinger, M., Wolff, M.J., 2001. Martian dust storms: 1999 Mars Orbiter Camera observations. J. Geophys. Res. 106, 23653–26687.

Hapke, B., 1986. Bidirectional reflectance spectroscopy. 4. Extinction and the opposition effect. Icarus 67, 264–280.

Hartsfeld, N., Ringel, G., 2003. Pearls in Graph Theory: A Comprehensive Introduction. Dover, pp. 272.

Hinson, D.P., Wang, H., 2010. Further observations of regional dust storms and baroclinic eddies in the northern hemisphere of Mars. Icarus 206 (1), 290–305. http://dx.doi.org/10.1016/j.icarus.2009.08.019.

Hinson, D.P., Wang, H., Smith, M.D., 2012. A multi-year survey of dynamics near the surface in the northern hemisphere of Mars: Short-period baroclinic waves and dust storms. Icarus 219 (1), 307–320. http://dx.doi.org/10.1016/j.icarus.2012.03.001.

Hollingsworth, J.L., Kahre, M.A., 2010. Extratropical cyclones, frontal waves and Mars dust: Modeling and considerations. Geophys. Res. Lett. 37, L22202. http://dx.doi.org/10.1029/2010GL044262.

Kahn, R.A., Martin, T.Z., Zurek, R.W., Lee, S.W., 1992. The martian dust cycle. In: Kieffer, H. et al. (Eds.), Mars. Univ. of Ariz. Press, Tucson, pp. 1017–1053.

Kahre, M.A., Murphy, J.R., Haberle, R.M., 2006. Modeling the martian dust cycle and surface dust reservoirs with the NASA Ames general circulation model. J. Geophys. Res. 111, E6. http://dx.doi.org/10.1029/2005JE002588.

Kleinboehl, A. et al., 2009. Mars Climate Sounder limb profile retrieval of atmospheric temperature, pressure, and dust and water ice opacity. J. Geophys., Res. 114, E10006. http://dx.doi.org/10.1029/2009JE003358.

Liu, J.J., Richardson, M.I., Wilson, R.J., 2003. An assessment of the global, seasonal, and interannual spacecraft record of martian climate in the thermal infrared. J. Geophys. Res. 108 (E8), 5098. http://dx.doi.org/10.1029/2002JE001921.

Martin, T.Z., 1986. Thermal infrared opacity of the Mars atmosphere. Icarus 66 (1), 2–21. http://dx.doi.org/10.1016/0019-1035(86)90003-5.

Martin, T.Z., Richardson, M.I., 1993. New dust opacity mapping from Viking Infrared Thermal Mapper data. J. Geophys. Res. 98 (E6), 10941–10949. http://dx.doi.org/10.1029/93JE01044.

Martin, L.J., Zurek, R.W., 1993. An analysis of the history of dust storm activity on Mars. J. Geophys. Res. 98, 3221–3246.

Mulholland, D.P., Read, P.L., Lewis, S.R., 2013. Simulating the interannual variability of major dust storms on Mars using variable lifting thresholds. Icarus 223, 344–358.

Newman, C.E., Lewis, S.R., Read, P.L., Forget, F., 2002. Modeling the martian dust cycle. 2. Multiannual radiatively active dust transport simulations. J. Geophys. Res. 107. http://dx.doi.org/10.1029/2002JE001920.

Smith, M.D., 2004. Interannual variability in TES atmospheric observations of Mars during 1999–2003. Icarus 167, 148–165.

Smith, M.D., 2008. Spacecraft observations of the martian atmosphere. Annu. Rev. Earth Planet. Sci. 36, 191–219. http://dx.doi.org/10.1146/annurev.earth.36.031207.124335.

Smith, M.D., 2009. THEMIS observations of Mars aerosol optical depth from 2002 to 2008. Icarus 202, 444–452. http://dx.doi.org/10.1016/j.icarus.2009.03.027.

Smith, M.D., Conrath, R.J., Pearl, J.C., Christensen, P.R., 2002. Thermal Emission Spectrometer observations of martian planet-encircling dust storm 2001A. Icarus 157 (1), 259–263. http://dx.doi.org/10.1006/icar.2001.6797.

Strausberg, M.J., Wang, H., Richardson, M.I., Ewald, S.P., 2005. Observations of the initiation and evolution of the 2001 Mars global dust storm. J. Geophys. Res. 110 (E2), E02006. http://dx.doi.org/10.1029/2004JE002361.

Toigo, A.D., Richardson, M.I., Wilson, R.J., Wang, H., Ingersoll, A.P., 2002. A first look at dust lifting and dust storms near the south pole of Mars with a mesoscale model. J. Geophys. Res. 107, E7. http://dx.doi.org/10.1029/2001JE001592. Art. No. 5050.

Toigo, A.D., Lee, C., Newman, C.E., Richardson, M.I., 2012. The impact of resolution on the dynamics of the martian global atmosphere: Varying resolution studies

with the MarsWRF. Icarus 222 (1), 276–288. http://dx.doi.org/10.1016/j.icarus.2012.07.020.
Wang, H., 2007. Dust storms originating in the northern hemisphere during the third mapping year of Mars Global Surveyor. Icarus 189 (2), 325–343. http://dx.doi.org/10.1016/j.icarus.2007.01.014.
Wang, H., Ingersoll, A.P., 2002. Martian clouds observed by Mars Global Surveyor Mars Orbiter Camera. J. Geophys. Res. 107 (E10), 5078. http://dx.doi.org/10.1029/2001JE001815.
Wang, H., Richardson, M.I., Wilson, R.J., Ingersoll, A.P., Toigo, A.D., 2003. Cyclones, tides, and the origin of a cross-equatorial dust storm on Mars.
Wang, H., Zurek, R.W., Richardson, M.I., 2005. Relationship between frontal dust storms and transient eddy activity in the northern hemisphere of Mars as observed by Mars Global Surveyor. J. Geophys. Res. 110 (E7). http://dx.doi.org/10.1029/2005JE002423.
Wang, H., Toigo, A.D., Richardson, M.I., 2011. Curvilinear features in the southern hemisphere observed by Mars Global Surveyor Mars Orbiter Camera. Icarus 215 (1), 242–252. http://dx.doi.org/10.1016/j/icarus.2011.06.029.
Wang, H., Richardson, M.I., Toigo, A.D., Newman, C.E., 2013. Zonal wavenumber three traveling waves in the northern hemisphere of Mars simulated with a general circulation model. Icarus 223 (2), 654–676. http://dx.doi.org/10.1016/j.icarus.2013.01.004.
Wilson, R.J., Hamilton, K., 1996. Comprehensive model simulation of thermal tides in the martian atmosphere. J. Atmos. Sci. 53 (9), 1290–1326.